Investigation into Instantaneous Centre of Rotation for Enhanced Design of Floating Offshore Wind Turbines

Katarzyna Patryniak[1], Maurizio Collu[1], Jason Jonkman[2], Matthew Hall[2], Garrett Barter[2], Daniel Zalkind[2], and Andrea Coraddu[3]

[1]Department of Naval Architecture, Ocean and Marine Engineering, University of Strathclyde, Glasgow, UK
[2]National Renewable Energy Laboratory, Golden, CO, USA
[3]Faculty of Mechanical, Maritime and Materials Engineering, Delft University of Technology, Delft, Netherlands

Correspondence: Katarzyna Patryniak (katarzyna.patryniak@strath.ac.uk)

Abstract. The dynamic behaviour of Floating Offshore Wind Turbines (FOWT) involves complex interactions of multivariate loads from wind, waves, and currents, which result in complex motion characteristics. Although methods for analysing global motion responses are well-established, the time- and location-dependent kinematics remain underexplored. This paper investigates the Instantaneous Centre of Rotation (ICR), a point of zero velocity at a time instance of general plane motion.

5   Understanding and strategically positioning the ICR can reduce the dynamic motion in critical structural locations, enhancing the performance and structural robustness of FOWTs. The paper presents a method for computing the ICR using time domain simulation results and proposes a statistical analysis approach suitable for design studies. Building on prior research, it examines the sensitivity of the ICR to external loading and design features, providing insights into how these factors influence motion response and how the motion response influences the statistics of the ICR, structural loads, and other performance

10   metrics of interest. The study explores two FOWT configurations, a spar and a semisubmersible, identifying design variables that most effectively control the ICR statistics and identifying the ICR statistics most correlated with the responses of interest. Finally, through two case studies, we demonstrate how to apply these new insights in a practical design scenario. By adjusting the design variables most correlated with the ICR (fairlead vertical position and centre of mass for the spar, and mooring line length and heave plate diameter for the semisubmersible), we successfully modified the designs of the floating support

15   structures to reduce the loads in the mooring lines, tower base, and blade roots, improving the ultimate strength and fatigue characteristics as compared to the original designs.

1   Introduction

The dynamic behaviour of Floating Offshore Wind Turbines (FOWTs) presents significant complexity due to the diverse range of multivariate loads they encounter in an offshore environment. The distinctly distributed inertial, hydrostatic, mooring, and

20   aero- and hydrodynamic loads are influenced by varying combined wind, wave, and current impacts. This results in response characteristics unique to FOWTs and not observed in other offshore structures. Although the methods for analysing the global motion responses of FOWTs are well established, the intricate, time- and location-dependent kinematics and motion patterns remain underexplored.

As highlighted by Patryniak et al. (2023), when a FOWT undergoes general plane motion, one can identify a point, known as
the Instantaneous Centre of Rotation (ICR), where the velocity is zero at a given moment. This point is not necessarily located
within the physical boundaries of the FOWT and is highly dynamic, shifting in response to changing environmental loads and
the resulting platform motions. Accurate identification of the ICR and its statistics can offer valuable insights for optimising
motion reduction strategies and enhancing the FOWT's performance and structural robustness. By strategically modifying
design elements to influence the position of the ICR, it is possible to minimise dynamic motions at critical locations. For
example, aligning the fairleads with the ICR could limit the dynamic part of the motion that does not contribute to useful
restoring but does contribute to fatigue damage of the mooring lines. Similarly, positioning the ICR near the Rotor-Nacelle
Assembly (RNA) could decrease rotor and nacelle motion, reducing aerodynamic load fluctuations and mitigating fatigue
across the system.

Early studies on the center of rotation of floating structures were conducted by Stewart and Ewers (1979) and Standing
(1991), focusing on barge vessels. Both authors noted significant oscillations in the centre of rotation, with Standing observing
that the point "tends to wander wildly" in irregular waves. This work challenged the assumption that the centre of rotation
is aligned with the centre of gravity, and highlighted the importance of hydrodynamic loads. Haslum and Faltinsen (2000)
further examined the center of rotation in a spar platform undergoing surge-pitch motion, revealing its sensitivity to oscillation
frequency and fairlead location. Souza et al. (2012) introduced an experimental method to determine the instantaneous centre
of rotation (ICR) using velocity vectors from two probes on the floating body. Fernandes et al. (2016) and Costa et al. (2018)
built on the previous work by analysing an FPSO vessel in regular waves, showing that the ICR locus (a curve formed by
all ICR points) is a straight line that does not align with the vessel's symmetry and varies with wave frequency. At very low
frequencies, the ICR exhibited a behaviour akin to pure translation, approaching an infinite distance above the body. Costa
et al. (2020a) found that the ICR coordinates of a moored vessel in regular head waves, free to move in surge, heave, and
pitch, closely follow a Cauchy distribution. In subsequent work (Costa et al., 2020b), the authors expanded their investigation
to oblique seas and six degrees of freedom, further reaffirming the ICR's dependence on external loading frequency.

Despite its relevance, the ICR has not been a focal point in FOWT studies. A few examples include the work by Eliassen
(2015), which was the first attempt to investigate the centre of rotation of a FOWT without presupposing its location, and the
study by Kaptan et al. (2022), which examined the influence of wave frequency on the centre of rotation for two different
floating concepts. Lemmer et al. (2020) considered the centre of rotation as the point where the surge and pitch Response
Amplitude Operators combine to produce near-zero motion. The authors utilised taut mooring semisubmersible designs to
ensure that the system rotates about the hub, thereby achieving preferable dynamic response characteristics, improved power
quality, and reduced tower base loads. While the location of the centre of rotation was determined through frequency domain
analysis, its instantaneous nature was not taken into account.

The concept of ICR in the context of FOWTs was most recently explored by Patryniak et al. (2023). The study provided
a comprehensive explanation of the ICR concept, developed a method for calculating the ICR of FOWTs through eigenanal-
ysis and in the time domain, and analysed its time history and statistical behaviour for a specific case involving a Hywind
spar (Jonkman, 2010) with the NREL 5MW reference rotor (Jonkman et al., 2009), subjected to regular and irregular waves

of varying frequencies and amplitudes. The findings indicated that the ICR of a FOWT is influenced by the frequency of the
incident waves and, at low frequencies, is also affected by wave height. Although significant insight into the ICR behaviour
was provided, only one floating structure was investigated, and realistic environmental conditions (combined wind, wave, and
current load) were not considered, limiting the applicability of the study.

In this work, we build on the previously developed method and further explore the ICR for FOWT design variations under
complex loading conditions typical of operational FOWTs to incorporate this knowledge into the design process. We begin
by examining the influence of more complex environmental loading conditions (Sect. 3) to enhance understanding of ICR
behaviour in realistic operational scenarios. For ICR insights to be useful in the design process, two conditions must be met.
First, the ICR must be correlated with FOWT responses that are critical for design improvement. Second, a set of design
variables that can be adjusted to "control" the ICR statistics must be identified to enable these improvements. Accordingly, in
Sect. 4, we explore how specific design decisions affect ICR behaviour, followed by an investigation of the relationship between
the ICR and key FOWT responses (Sect. 5). This sensitivity analysis helps identify key design features that can be prioritised
during the FOWT optimisation process. The findings of this paper can be readily applied in a practical design scenario, as will
be demonstrated in Sect. 6.

2 Methodology

The objectives of this study are: i) to understand the behaviour of the ICR in a complex, realistic environment, and ii) to
demonstrate how knowledge of ICR behaviour can be leveraged to improve FOWT designs. The ICR can serve as a useful
metric in the FOWT design process, provided that:

1. The FOWT design can be modified in ways that influence the ICR statistics,

2. The ICR statistics significantly affect the responses of interest (i.e., the performance of the FOWT).

Therefore, to enable a practical application of the new knowledge about the ICR of FOWTs, this study examines the rela-
tionships among design variables, ICR statistics, and response statistics. In particular, we investigate which design variables
are significantly correlated with the ICR statistics and which ICR statistics are significantly correlated with the responses of
interest. The procedure followed is illustrated in Figure 1, as outlined below and detailed in the subsequent sections.

The study begins with one-at-a-time perturbations of multiple design variables, which are features of the floating platform
and mooring system. This approach allows for the examination of correlations with ICR statistics (mean and standard deviation
of horizontal and vertical ICR components). Although more comprehensive experimental designs, such as Full Factorial or
Latin Hypercube, offer deeper insights into design space behaviour, perturbing one variable at a time while keeping all other
variables at their original design values significantly reduces the design space size, keeps the computational cost tractable, and
allows for clear presentation and interpretation of the results.

Once the relationships between the design variables and ICR are established, the most impactful parameters are identified
for downselection. These parameters are then subjected to a more thorough sensitivity analysis using a Full Factorial approach.
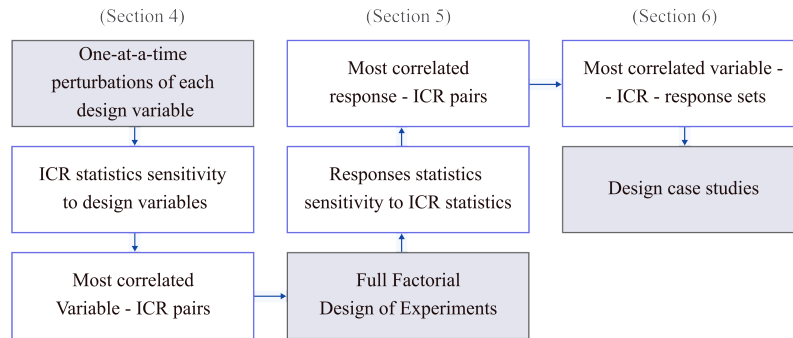
Figure 1. The procedure for investigation of the relationships between the design variables, ICR and responses statistics.

This analysis explores the relationships between all combinations of the selected parameters and the responses of interest (i.e., design performance metrics).

At this stage, highly correlated pairs of design variables and ICR statistics are further refined to include only those that also show strong correlations with the responses of interest. This systematic procedure helps identify design directions that may lead to significant improvements in the performance of the FOWTs through changes to ICR statistics.

The methods for computing the ICR and its statistics are outlined below.

2.1 Instantaneous Centre of Rotation derivation

When exposed to colinear unidirectional wind, wave, and current loads, FOWTs undergo general plane motion, with translational and rotational characteristics dependent on the external load and design of the structure (Patryniak et al., 2023). In particular, the centre of the pitch rotation depends on the amplitudes, frequencies, phases, and distributions of the external dynamic forces, and, therefore, its determination is nontrivial.

A point (not necessarily within the body) of zero velocity at a particular instant in time (i.e., ICR) can be found by analysing the velocity vectors at two arbitrarily chosen points on the body. While, by definition, the ICR appears to be instantaneously at rest, all other points in the body present pure rotation about this point, i.e., follow circular paths around the ICR (Meriam and Kraige, 1993). Therefore, the ICR can be found at the intersection of the perpendiculars to the velocities of the two points (A and B in Figure 2), assuming a rigid body. In the special case when the velocity vectors are parallel and do not cross, and the line joining points A and B is perpendicular to the velocities, the ICR can be obtained through a direct proportion (Meriam and Kraige, 1993), as illustrated in the middle subfigure of Figure 2. In the special case of pure translation (right subfigure of Figure 2), the ICR tends to infinity. The vectors required for this calculation can be found by measuring the velocities in A and B, as obtained from the time-domain numerical simulations (detailed in Sect. 2.3).

Note that the location of the ICR changes as the body moves or loading conditions change, both in terms of the body-fixed and global inertial coordinate systems, and therefore, it only exists at a particular instant in time (hence "instantaneous"). As shown previously by Patryniak et al. (2023) and reiterated here in Figure 3, in regular waves (a purely theoretical condition), the
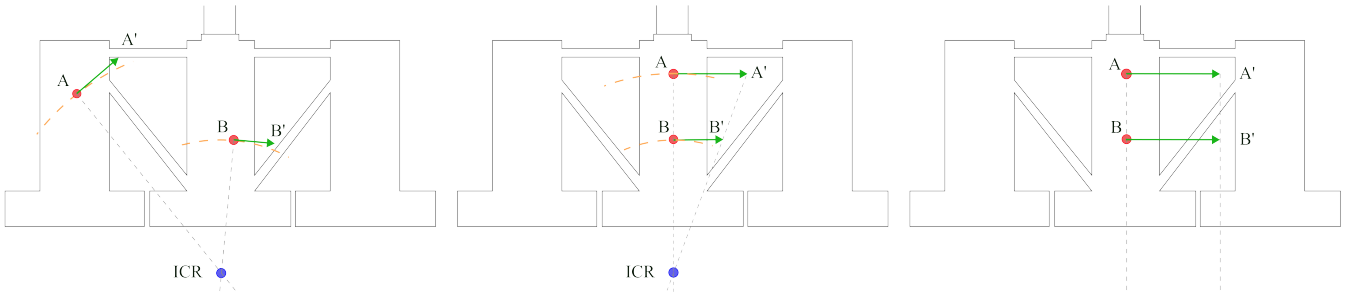
Figure 2. Construction of the ICR using velocity vectors at two points on the floating body. Left: general case - misaligned nodes, middle: special case - aligned nodes, right: special case - pure translation.

ICR coordinates exhibit a distinctive time history pattern. When the pitch displacement reaches its minimum or maximum, the
115   pitch velocity is zero (pure translation), and the ICR tends toward infinity. At other times, it concentrates around finite locations. The phases before and after each pitch extremum result in the ICR clustering around unique points, as also illustrated in the histograms of Figure 6. In a more complex, stochastic environment, such a regular pattern cannot be observed (Figure 4). However, still, ICR coordinates follow a well-defined distribution illustrated in Figure 5.
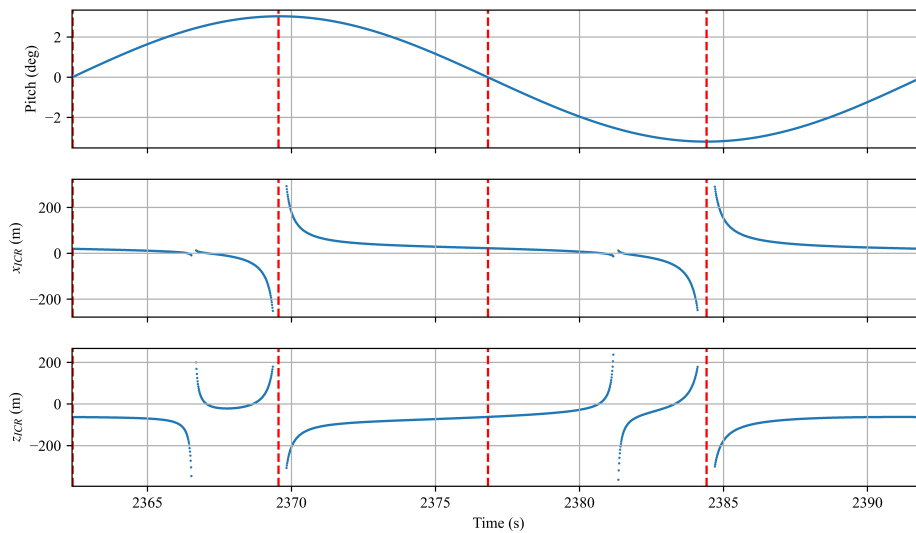
Figure 3. ICR time history during one period of pitch motion. Reproduced from (Patryniak et al., 2023).

2.2 Instantaneous Centre of Rotation statistics

120   Given that the Instantaneous Centre of Rotation (ICR) can exhibit asymptotic behaviour and is very irregular under stochastic environmental loading conditions, analysing time-domain signals directly can be difficult and not readily applicable in the
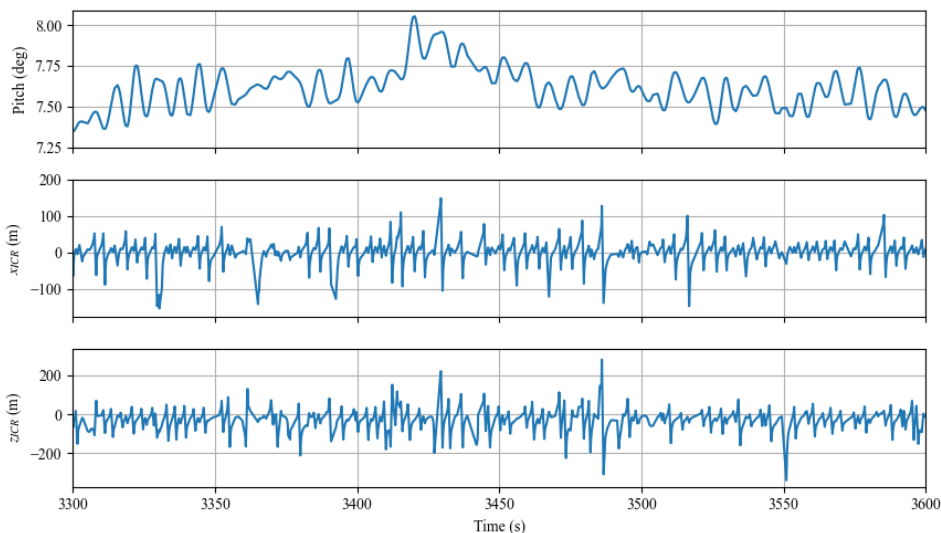
Figure 4. ICR time history during platform motion in a realistic environmental condition.
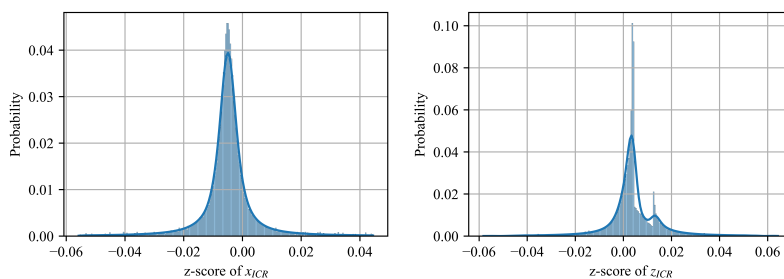
Figure 5. Histogram of ICR coordinates for a FOWT in regular waves.
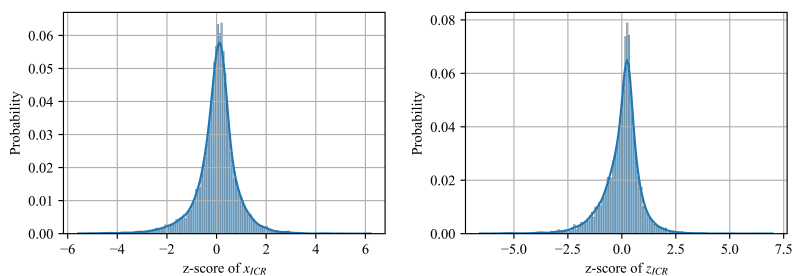
Figure 6. Histogram of ICR coordinates for a FOWT in a realistic environmental condition.

design context. Therefore, a statistical analysis approach is followed instead. In particular, the distribution characteristics of the in-plane coordinates of the ICR (type, mean, standard deviation, skewness and kurtosis) are investigated.

One-sample Kolmogorov-Smirnov (K-S) test with hypothesis testing is performed to establish whether the ICR follows
a normal distribution. This test compares data sampled from a fitted normal distribution with the samples from the original
data and outputs two metrics: the K-S statistic, which measures the maximum discrepancy between the empirical cumulative
distribution functions of the two samples, and the p-value, which indicates the probability of observing the test results under
the null hypothesis. The null hypothesis is that the two samples come from the same distribution. A high p-value above
the significance level of 0.05 suggests insufficient evidence to state that the two samples come from different distributions.
Therefore, a low K-S value and p-value above 0.05 are needed to confirm that the data closely follows normal distribution.

When studying the relationships between the design variables, ICR, and FOWT responses, Spearman correlation coefficients
are calculated using Eq. 1:

$$\rho = 1 - \frac{6 \sum_{i=1}^{n} d_i^2}{n(n^2 - 1)} \tag{1}$$

d_i is the difference between the ranks[1] of each pair, and n is the number of observations (here, simulations). The correlation
scores close to 1 or -1 indicate a strong monotonic (not necessarily linear) relationship without making any assumptions about
the data distribution. Note that the correlation scores do not provide any information about the causal relationship between the
variables.

2.3 Dynamic simulations

All simulations in this study are performed with OpenFAST - a state-of-the-art, extensively validated nonlinear aero-hydro-
servo-elastic coupled time-domain model of dynamics (NREL, 2024). The degrees of freedom include six rigid body motion
modes; although possible in OpenFAST, the elastic dynamics are not modelled in this study, as the analysis relies on a rigid
body assumption. The NREL 5-MW baseline variable-pitch variable-speed controller allows for blade pitch and rotor speed
variations depending on the mean wind speed and slight rotor speed variations due to the system motion. The aerodynamic
solution relies on the Blade-element Momentum theory with Beddoes-Leishman unsteady blade airfoil aerodynamics model,
tip and hub loss corrections, and tower influence based on the potential flow. The 1st-order hydrodynamics of the spar and
semisubmersible platforms are modelled through frequency-to-time-domain transforms based on the potential coefficients
obtained from the Boundary Element Method (BEM) code WAMIT (Lee and Newman, 2006) (2nd-order hydrodynamics are
not modelled). Viscous loads are computed from Morison's theory. The nonlinear mooring loads are computed using a lumped-
mass mooring line model MoorDyn (Hall and Goupee, 2015). The model includes the effects of axial stiffness and damping,
weight and buoyancy, hydrodynamic viscous forces, and vertical spring-damper forces from contact with the seabed.

In this work, the design variations involving a change of the underwater shape of the floating platform are kept small to avoid
the need for repeated solution of the potential coefficients, which is computationally expensive. For large-volume structural
members, this may still impact the accuracy of the solution. Therefore, the results in this paper are interpreted assuming no
change in potential hydrodynamic loads.

---

[1]A rank is the position of a value within a sorted list of data points, ordered from smallest to largest

Sect. 3 explores the ICR under various synthetic environmental conditions. Instead of relying on the predefined design load cases (e.g., DLC 1.6, which involves an operational turbine in severe sea state, and DLC 6.1, which considers a parked turbine experiencing severe wind and sea conditions, as outlined in the IEC 61400-3-2 standard (IEC, 2019)), this study selectively applies different loading components. This approach aims to provide deeper insights into the ICR behaviour related to specific sources of loading. The wind conditions are characterised by the mean hub-height wind speed, profile (shear), and turbulence intensity, and the wave conditions (sea state) are characterised by the (significant) wave height and (peak) period. Wind and wave directions are aligned with the positive x-axis (no misalignment is considered in this paper). The wave peak-shape parameter is not varied; its value is adjusted based on the peak period and significant wave height, as recommended in the IEC 61400-3 Annex B (IEC, 2009).

Sect.s 4 and 5, on the other hand, investigate ICR over a range of realistic environmental conditions. Each design variant is simulated in 10 environmental conditions, listed in Table 1, representing binned metocean data obtained for the Scottish sectoral marine plan "NE8" (these bins account for $98.4\,\%$ of cumulative probability). The responses presented in this paper refer to the average responses weighed with the probability of each of the 10 conditions. Each simulation is run for $1\,\mathrm{hour}$ (excluding the initial transient phase) with a single random seed.

Table 1. Environmental conditions binning. Wind shear fixed at 0.2 and turbulence intensity at $14\,\%$.

Condition	1	2	3	4	5	6	7	8	9	10
V_s (m/s)	4.1	6.3	8.5	10.7	12.9	15.1	17.3	19.5	21.7	23.9
H_s (m)	1.09	1.23	1.44	1.75	2.17	2.68	3.27	3.95	4.71	5.42
T_p (s)	8.68	8.54	8.14	7.65	7.51	7.63	8.04	8.58	9.16	9.58
Probability	0.087	0.213	0.266	0.230	0.134	0.052	0.013	0.002	0.001	0.001

2.4 Coordinate systems

This study employs two distinct coordinate systems. The global inertial coordinate system, illustrated in Figure 16, offers a reference frame for examining how the ICR responds to varying environmental loading conditions and design parameters. By remaining unaffected by the structural displacements, it provides a clear view of how external forces influence the ICR. It is centred at the intersection of the mean waterline and the undisplaced tower axis (centroid of the undisplaced initial waterplane area). Conversely, the body-fixed coordinate system is used for design-focused evaluations, where the goal is to position the ICR relative to specific locations on the floating structure. This system initially coincides with the global inertial coordinate system but moves (both translates and rotates) with the floating body. Across the paper, the results are primarily presented in the global inertial frame. The local frame supports the interpretation of the observed design trends (distinction will be made where appropriate).

3 Environmental conditions effect

180 In a previous study (Patryniak et al., 2023), the ICR of FOWTs was only studied in regular waves, which provided a limited understanding of the behaviour in real operational scenarios. Therefore, this test aims to establish the dependence of the ICR on more complex environmental loading conditions, to understand the factors driving the ICR, and to establish the applicability of the ICR as a design metric.

3.1 Study setup

185 The sensitivity of the ICR to environmental loading conditions is studied through a series of simulations of gradually increasing complexity, as outlined in Table 2. All simulations are run for the case of the original design of the OC3 Hywind spar (Jonkman, 2010) with the 5MW reference rotor (Jonkman et al., 2009) as the example system.

Table 2. Impact of varied environmental loading on the ICR - conditions considered.

	Wind				Waves			Current
Group	Type	V_s	TI	Shear	Type	H_s	T_p	V_c
(-)	(-)	(m/s)	(-)	(-)	(-)	(m)	(s)	(m/s)
A	-	-	-	-	Reg	1.87	5-17.0	-
B	-	-	-	-	JONSWAP	1.87	7.47	-
C	Steady	3-25	-	0.2	Reg	1.87	7.47	-
D	Steady	11.4	-	0.1-0.4	Reg	1.87	7.47	-
E	Turbulent	11.4	0.1-0.3	0.2	Reg	1.87	7.47	-
F	-	-	-	-	Reg	1.87	7.47	0.5-1.2
G	Turbulent	11.4	0.17	0.2	JONSWAP	1.87	7.47	0.85

First, a simple test in regular waves is performed for a wide range of wave periods (or frequencies), keeping the wave height fixed (group A in Table 2), Subsequently, the response in irregular waves is simulated, keeping the peak period and significant 190 wave height at the previously set values (group B). Irregular sea state includes the component waves at various frequencies, with the most energy content around the peak frequency and contributions from lower and higher frequency waves. The complexity is then increased by including the effect of steady wind (from cut-in to cut-out), which puts the FOWT into a new equilibrium position (group C), as well as the effect of the wind shear, which affects the vertical distribution of the wind load (group D). Group E simulations are run in the rated wind speed condition, this time with turbulent wind inflow of varying turbulence 195 intensity. The turbulent wind is expected to increase the dynamic responses at very low frequencies not excited otherwise (the second-order wave loads are not modelled). Group F adds the effect of the current. Finally, group G represents the condition likely encountered by an operational FOWT, including the combined effects of the stochastic wind, wave, and current loads.

The results obtained for each group will be presented in turn - all results are given in the global inertial coordinate system.

3.2 Results

200 The simulations conducted under Group A environmental conditions (regular waves) are analysed to understand how the external load period (or frequency) influences the motion behaviour and the ICR of the floating system. As presented in Figure 7 and Table 3, the mean of the x-coordinate of ICR remains around zero regardless of the wave period, and the mean of the z-coordinate approaches zero as the wave period increases. As the wave period increases (which corresponds to a decrease in frequency), the distribution of z_{ICR} becomes wider (higher standard deviation). This happens because as the wave period

205 increases, the waves become longer and approach the system's surge and heave natural periods ($125\,\mathrm{s}$ and $31\,\mathrm{s}$, respectively), resulting in increased dynamic surge and heave motion of the platform. Figure 8 illustrates that, for a given rotational velocity, if a significant horizontal translational velocity is superimposed, the ICR, defined as the point where normals to the velocity vectors intersect, shifts either higher or lower depending on the direction of the translation direction and the instant of the periodic motion (i.e., the phase difference between the translation and rotation). Similarly, larger vertical velocity shifts the

210 ICR horizontally away from the platform. This results in both lower and higher values of the ICR, thereby widening the distributions as observed.
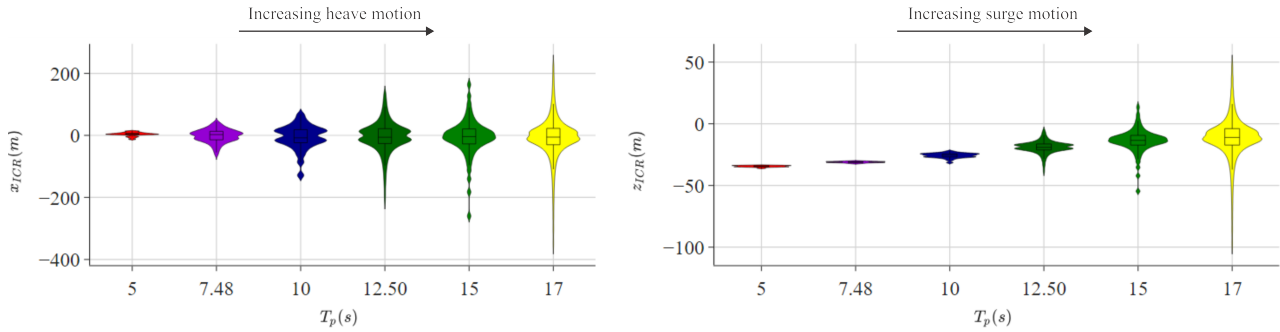
Figure 7. Effect of the regular waves period on the distribution of ICR coordinates (group A).

Table 3. The ICR of a FOWT in regular waves (group A).

	Surge		Heave		x_{ICR}		z_{ICR}	
T	mean	std	mean	std	mean	std	mean	std
(s)	(m)	(m)	(m)	(m)	(m)	(m)	(m)	(m)
5.00	-0.09	0.07	0.02	0.00	3.55	6.28	-34.52	0.63
7.47	-0.10	0.21	0.02	0.02	-1.70	21.49	-31.12	0.61
10.00	-0.09	0.38	0.02	0.05	-6.38	39.50	-25.79	1.94
12.50	-0.09	0.51	0.02	0.09	-4.77	51.61	-19.08	5.15
15.00	-0.09	0.62	0.03	0.14	-6.69	62.63	-13.90	10.08
17.50	-0.09	0.76	0.02	0.16	-6.85	70.59	-11.43	17.74
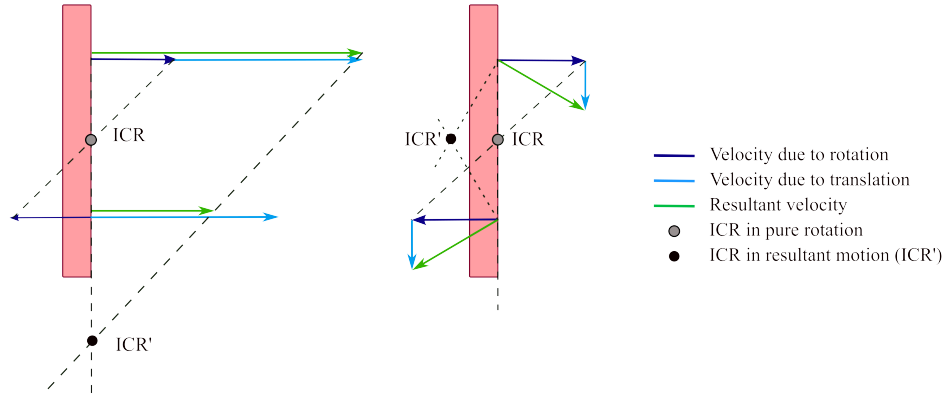
Figure 8. The effect of superposition of rotational and horizontal translational (left) and vertical translation (right) velocities on ICR position.

The simulations of Group C environmental conditions (steady wind) are analysed to understand how the magnitude of the non-fluctuating load applied at the rotor height influences the motion behaviour and the ICR of the floating system. The results presented in Table 4 and Figure 9 show that the mean of x_{ICR} increases with wind speed, while the mean of z_{ICR} follows a nonmonotonic trend. As seen previously for the regular wave cases, the distribution of the vertical coordinate gets wider as the wind speed increases.

215

Table 4. The ICR of a FOWT in steady wind (group C).

	Surge		Heave		x_{ICR}		z_{ICR}	
V_s	mean	std	mean	std	mean	std	mean	std
(m/s)	(m)	(m)	(m)	(m)	(m)	(m)	(m)	(m)
0.0	-0.08	0.20	0.02	0.03	-2.59	29.80	-20.25	1.07
3.0	2.46	0.20	-0.01	0.02	-1.27	19.78	-31.71	2.65
4.9	6.60	0.20	-0.06	0.02	-1.19	19.83	-31.76	6.18
6.7	12.90	0.20	-0.18	0.02	-0.29	19.70	-31.11	11.31
8.6	21.34	0.20	-0.42	0.03	1.17	19.39	-29.59	18.24
11.4	36.15	0.20	-1.13	0.03	4.16	20.05	-25.11	28.31

The next group of simulations (group D) was conducted with a fixed mean hub-height wind speed of 11.4 m/s, varying the power exponent of the power law wind profile (shear). As demonstrated in Figure 10, the distribution of x_{ICR} remains mostly unaffected by the wind profile, as explained by negligible changes to the vertical motion (refer to Table 5). However, z_{ICR} exhibits a strong dependence on the vertical distribution of wind. Notably, as the power exponent increases, the centre of application of the aerodynamic load (centre of effort) also shifts upward, resulting in a higher mean pitch angle. This change leads to two observable effects: i) an increase in pitch angle reduces the thrust coefficient, and ii) the rotor-averaged wind speed is altered. Depending on the trade-off between these two factors, the total aerodynamic thrust may be either lower or higher.

220
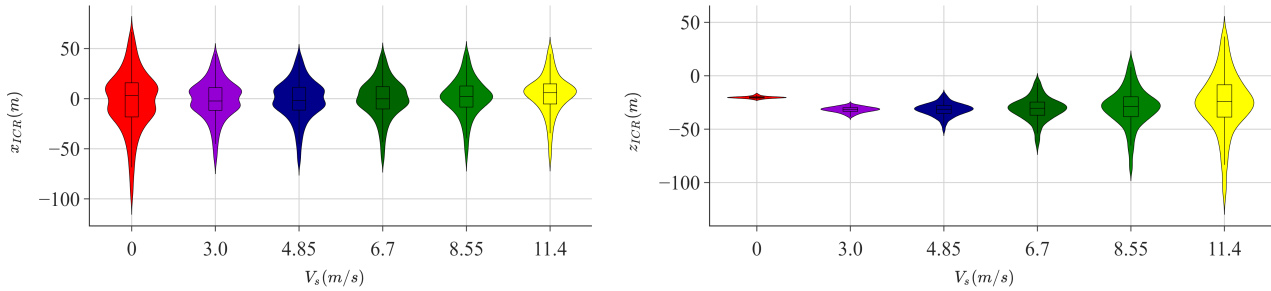
Figure 9. Effect of the steady wind speed on the distribution of ICR coordinates (group C).

This variation results in changes in the mean offset of the system, which subsequently affects the mooring loads, as observed in the previous tests. Subsequently, changes in the horizontal velocities of the FOWT influence the behaviour of z_{ICR}.

Table 5. The ICR of a FOWT in steady wind with shear (group D).

Shear	Surge mean	Surge std	Heave mean	Heave std	x_{ICR} mean	x_{ICR} std	z_{ICR} mean	z_{ICR} std
(-)	(m)	(m)	(m)	(m)	(m)	(m)	(m)	(m)
0.10	2.46	0.20	-0.01	0.02	-1.27	19.78	-31.71	2.65
0.15	12.90	0.20	-0.18	0.02	-0.29	19.70	-31.11	11.31
0.20	36.15	0.20	-1.13	0.03	4.16	20.05	-25.11	28.31
0.25	6.60	0.20	-0.06	0.02	-1.19	19.83	-31.76	6.18
0.30	21.34	0.20	-0.42	0.03	1.17	19.39	-29.59	18.24
0.35	35.93	0.20	-1.11	0.03	4.27	20.01	-25.59	28.96
0.40	35.95	0.20	-1.11	0.03	4.07	20.16	-25.49	28.88
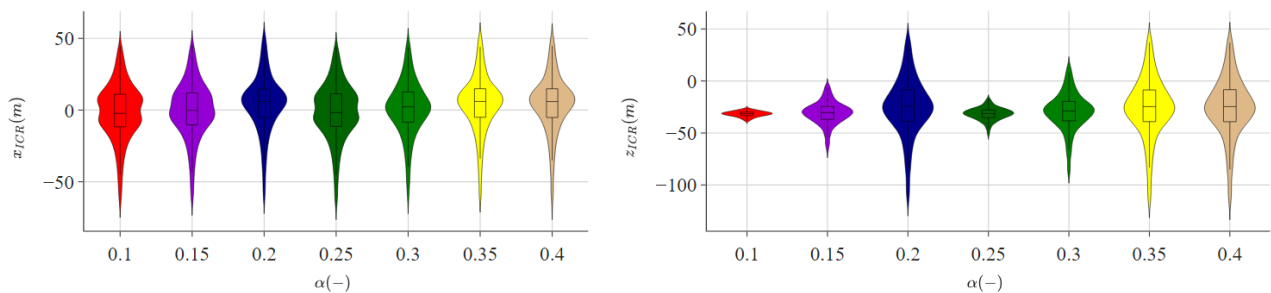
Figure 10. Effect of the wind shear on the distribution of ICR coordinates (group D).

225

Figures 11 – 12 and Tables 6 – 7 demonstrate that the ICR distribution does not significantly change in response to changing turbulence intensity (group E) or sub-surface current velocity (group F). The distributions at all turbulence levels remain normal, with a slightly increasing standard deviation due to increased horizontal load (higher turbulence intensity leads to

higher aerodynamic fluctuating load for any mean wind speed given). The current load on the slender cylinder of the spar floating structure is insignificant compared to other loads on the system.

Table 6. The ICR of a FOWT in turbulent wind (group E).

TI (%)	Surge mean (m)	Surge std (m)	Heave mean (m)	Heave std (m)	x_{ICR} mean (m)	x_{ICR} std (m)	z_{ICR} mean (m)	z_{ICR} std (m)
0	36.15	0.20	-1.13	0.03	4.16	20.05	-25.11	28.31
10	36.15	0.25	-1.13	0.04	4.11	20.26	-25.15	29.67
15	36.15	0.30	-1.13	0.04	3.77	20.33	-24.81	31.26
20	36.24	0.35	-1.14	0.05	3.84	20.92	-25.09	33.20
25	36.38	0.39	-1.15	0.05	3.93	21.37	-25.40	34.73
30	36.57	0.43	-1.16	0.06	3.63	22.13	-26.39	37.58
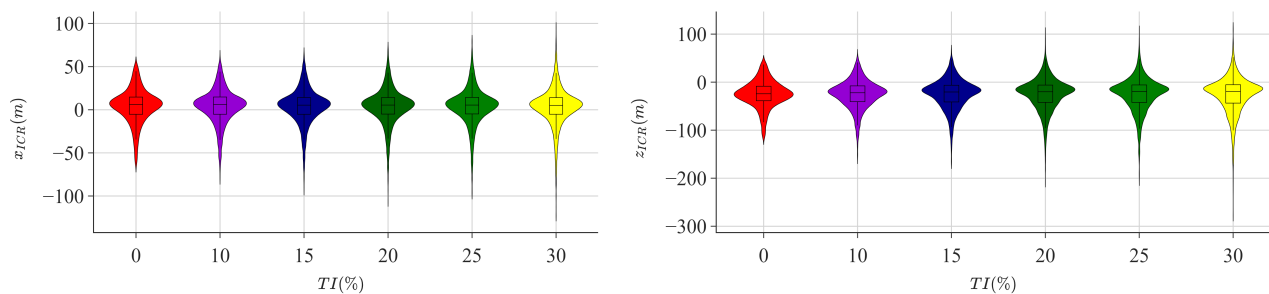
Figure 11. Effect of the turbulence intensity on the distribution of ICR coordinates (group E).

Table 7. The ICR of a FOWT simulated in varying current velocities (group F).

V_c (m/s)	Surge mean (m)	Surge std (m)	Heave mean (m)	Heave std (m)	x_{ICR} mean (m)	x_{ICR} std (m)	z_{ICR} mean (m)	z_{ICR} std (m)
0.00	-0.10	0.21	0.02	0.02	-1.55	21.39	-31.10	0.62
0.25	0.39	0.17	0.02	0.02	-1.36	19.34	-31.09	0.60
0.50	2.01	0.20	0.02	0.02	0.01	20.93	-31.17	0.66
0.70	3.94	0.20	0.01	0.02	-0.19	21.35	-31.18	0.82
0.80	5.27	0.20	0.01	0.02	-0.26	20.60	-31.23	0.91
1.00	8.41	0.21	-0.02	0.02	-0.35	23.20	-31.09	1.23
1.20	12.39	0.21	-0.07	0.02	-0.01	23.24	-31.16	1.60

230
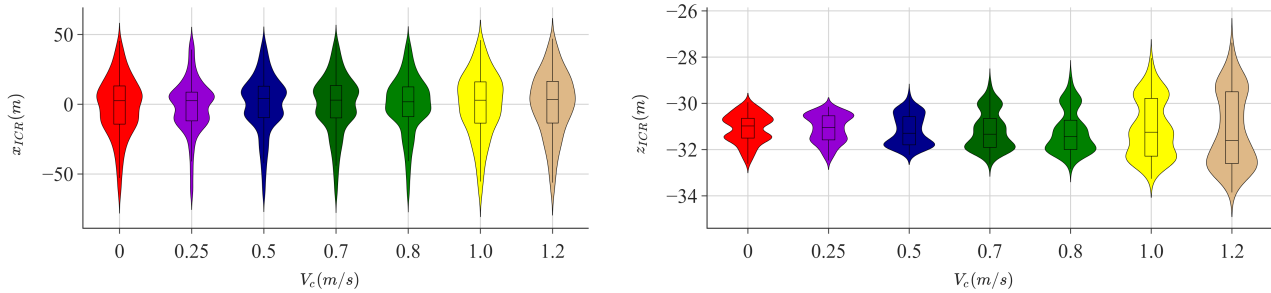
Figure 12. Effect of the current speed on the distribution of ICR coordinates (group F).

Finally, Figure 13 compares the distributions of the ICR coordinates of a FOWT placed in increasingly complex environmental conditions. While x_{ICR} appears consistent across all cases, the complexity of the loading significantly influences z_{ICR},
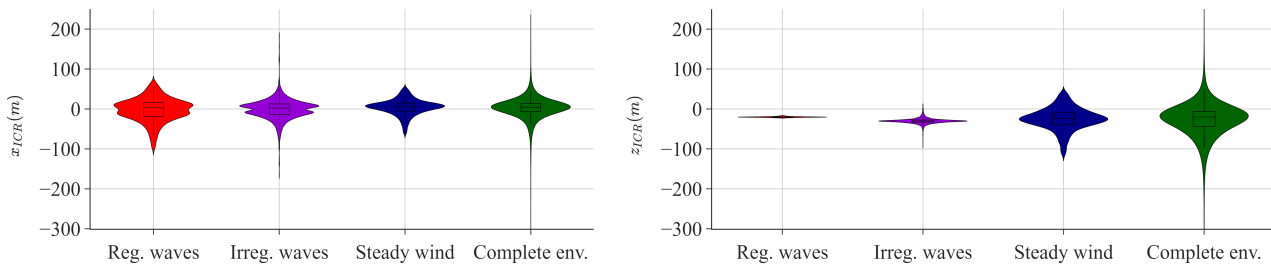
Figure 13. Effect of the increased environmental loading complexity on the distribution of ICR coordinates. The regular/irregular wave cases only include regular/irregular wave loads, the steady wind case includes steady wind in addition to irregular waves, and the complete environment includes irregular waves, turbulent wind, and current loads.

particularly in terms of its standard deviation. In the presence of regular waves, the vertical coordinate of ICR is confined to a narrow range. However, as irregular waves, wind, and current are gradually introduced, this range expands considerably.

235   Figure 14 provides a more detailed view of the effect of the environment complexity on z_{ICR} range. For each loading condition case, the confidence interval bounds were calculated using the mean and standard deviation of z_{ICR}, for various confidence levels. The ranges displayed in the figure represent the differences between the upper and lower bounds, indicating the intervals within which the true mean z_{ICR} is expected to lie with the specified confidence level. For any confidence level, more complex environmental loading leads to a broader range. This suggests that the complexity of the loading significantly

240   impacts the variability of z_{ICR} and the potential for extreme values. Importantly, broader ranges are also related to increased uncertainty in predicting the true mean of ICR, which may affect the usefulness of the ICR as a metric in the FOWT design process, as it is less likely to remain near a target location.

As reported in Table 8, the cases with no stochastic loads (i.e., regular wind and/or steady wind) show a relatively low K-S statistic and a high p-value (these metrics are introduced in Sect. 2.2), meaning that the ICR closely follows a normal

245   distribution in these scenarios. In contrast, the low p-value observed for the stochastic loading cases (irregular waves and/or
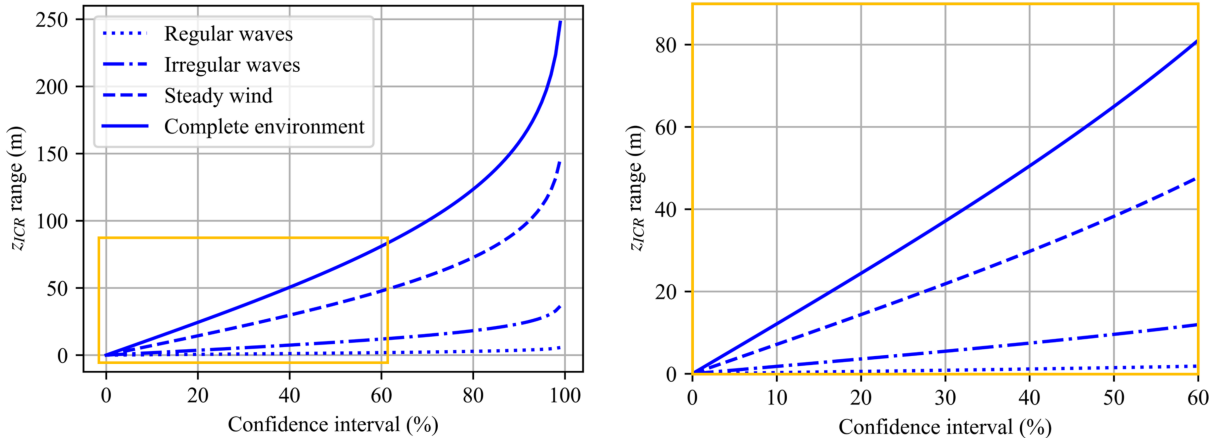
Figure 14. z_{ICR} range for different confidence intervals.

turbulent wind) suggests that we cannot reach the same conclusion regarding the normality of the ICR distribution in those instances. In those cases, the observed distribution of z_{ICR} has significantly increased skewness (more asymmetric) and excess

Table 8. The ICR of a FOWT under varying complexity environmental loading conditions. Each row represents one case of a group listed in Table 2.

Condition	Surge		Heave		x_{ICR}				z_{ICR}			
	mean (m)	std (m)	mean (m)	std (m)	mean (m)	std (m)	K-S (-)	p (-)	mean (m)	std (m)	K-S (-)	p (-)
Reg. waves (A)	-0.08	0.20	0.02	0.03	-2.59	29.80	0.11	0.58	-20.25	1.07	0.14	0.28
Irreg. waves (B)	-0.08	0.13	0.02	0.02	-1.04	25.52	0.10	0.72	-30.10	7.09	0.16	0.16
Steady wind (C)	36.15	0.20	-1.13	0.03	4.16	20.05	0.07	0.98	-25.11	28.31	0.12	0.46
Complete env. (G)	40.48	0.24	-1.38	0.03	2.28	29.23	0.13	0.34	-26.87	47.36	0.15	0.17

kurtosis (heavier tails and sharper peaks), as illustrated in Figure 15.

4 Design variables sensitivity

250 For any environmental loading condition, the motion response of different FOWT designs differs due to unique hydrostatic, hydrodynamic, mooring, and inertial characteristics. Therefore, this test investigates which design features (or variables) can be adjusted to achieve the desired ICR "location".

Two floating systems are considered in turn: a spar and a semisubmersible. The study includes four design variables common for both concepts: mooring line length, fairlead vertical position and radius, and platform centre of mass vertical position. 255 Additionally, there is one variable specific to the spar platform: waterline section diameter, and two variables specific to the
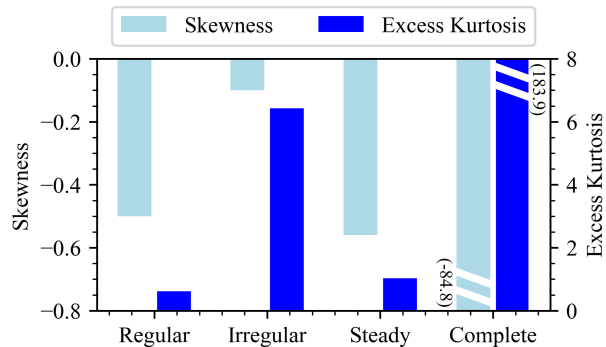
Figure 15. Skewness and kurtosis of z_{ICR} distribution for different environmental loading conditions.

semisubmersible platform: offset column and heave plate diameters. These are illustrated in Figure 16 and listed in Table 9. Note that this set of design variables is not exhaustive, and each parameter is varied independently. In particular, the fairlead position is adjusted without consideration of the floating platform dimensions, which keeps the effects isolated but neglects the proper physical interface between the fairleads and the platform. The catenary mooring line length is modified without altering the fairlead and anchor positions, resulting in changes to the line angle at the fairlead, the suspended line profile, and the portion of the line resting on the seabed. Likewise, the ratio between the offset column and heave plate diameters is not maintained when either variable is adjusted.

The broad range of design variables ensures that the study covers the entire design space, including some unconventional but realistic designs demonstrating a wide range of motion responses. Special attention was given to the mooring line length parameter, with the range chosen based on mooring pretension. Specifically, the study examined mooring line lengths that resulted in a $\pm 40\%$ variation in pretension compared to the original design, ensuring that realistic design variants are covered.

Note that these design variable perturbations may lead to a change in the mean heave of the floating platform (draft) that is not being rebalanced in this study (with the exception of the case study in Sect. 6, as will be explained). This effect may significantly affect the response of the FOWT and is considered when interpreting the results.

For each concept, the design variables were perturbed one at a time, and the change in the ICR statistics (in the global inertial coordinate system) was studied, as illustrated in Figure 17. The design variables presented in the figure were normalised to $0 - 1$ for clarity and unbiased comparison between the variables of different magnitudes. The absolute ranges of the variables are given in Table 9 for reference: note that these were purposefully selected to cover a very wide design space.

Based on the analysis of the spar platform in Figure 17, it is clear that variations in certain design variables significantly impact the position of the ICR. In particular, the results highlighted the significant influence of the centre of mass location on the ICR statistics. This effect was most evident for the z-coordinate (lower two plots), where the mean and standard deviation of the ICR showed strong negative and positive trends with the vertical position of the centre of mass, respectively. The vertical position of the fairlead was also found to be an important feature affecting the mean of x_{ICR}. The effects of other variables on
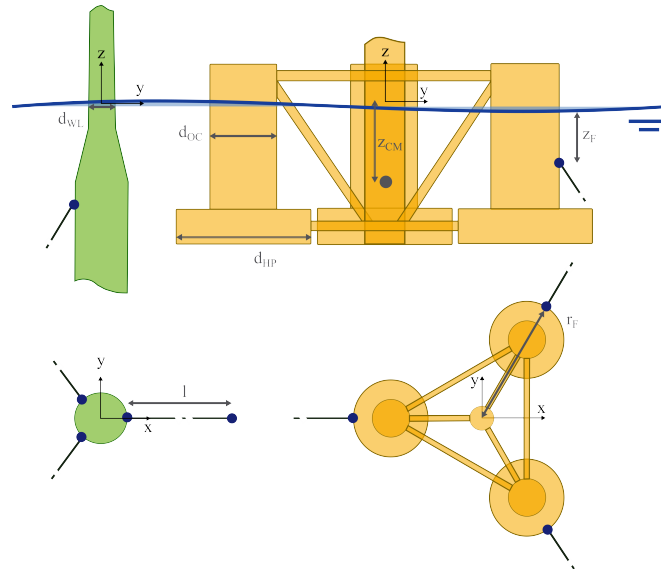
Figure 16. FOWT design variables. OC3 spar (left), OC4 semisubmersible (right).

Table 9. Original values and ranges of design variables. All values in (m).

	OC3 spar			OC4 semi		
	Original	Lower Bound	Upper Bound	Original	Lower Bound	Upper Bound
Line length (l)	902.2	891.6	924.1	835.5	828.5	850.0
Fairlead radius (r_F)	5.2	4.0	8.0	40.87	20.0	50.0
Fairlead z (z_F)	-70.0	-120	3.5	-14.0	-20.0	1.0
Platform CM (z_{CM})	-89.92	-110	-84.29	-8.66	-10.0	-7.0
Waterline D (d_{WL})	6.5	4.0	8.0	-	-	-
Offset column D (d_{OC})	-	-	-	12.0	10.0	14.0
Heave plate D (d_{HP})	-	-	-	24.0	19.33	27.35

the ICR metrics were relatively minor. Notably, no clear trends were observed for the standard deviation of x_{ICR}, suggesting
that the variables examined do not significantly influence this metric independently.

For the semisubmersible-type FOWT, Figure 18 demonstrates that the design variables have a more limited impact on the
ICR than was the case for the spar platform. Specifically, the mean position of the ICR remained within approximately $4\,\mathrm{m}$
across all design variations, indicating a smaller impact from design changes. Notably, the heave plate diameter emerged as
a significant parameter, affecting both the mean and the fluctuations in the ICR position. To a lesser degree, the mean x-
coordinate of the ICR was also responsive to changes in mooring line length, and the standard deviation of x_{ICR} showed a
positive trend with the fairlead radius. The influence of other design variables on the ICR was minor.
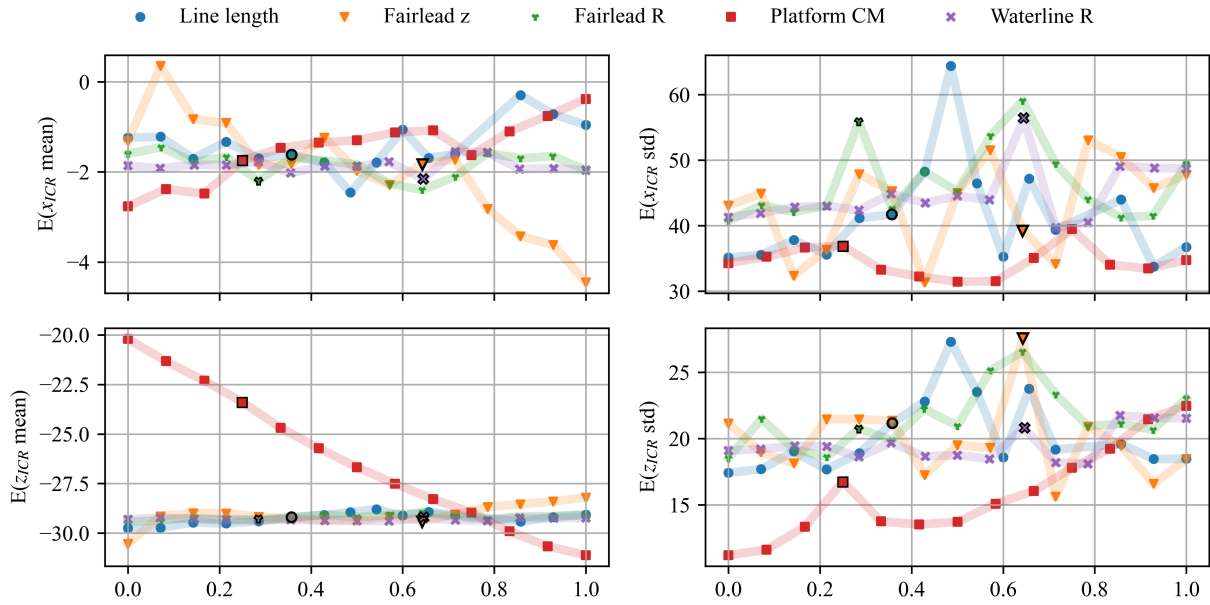
Figure 17. ICR statistics for different one-at-a-time design variable perturbations for a spar FOWT. Original design values marked with black outline.
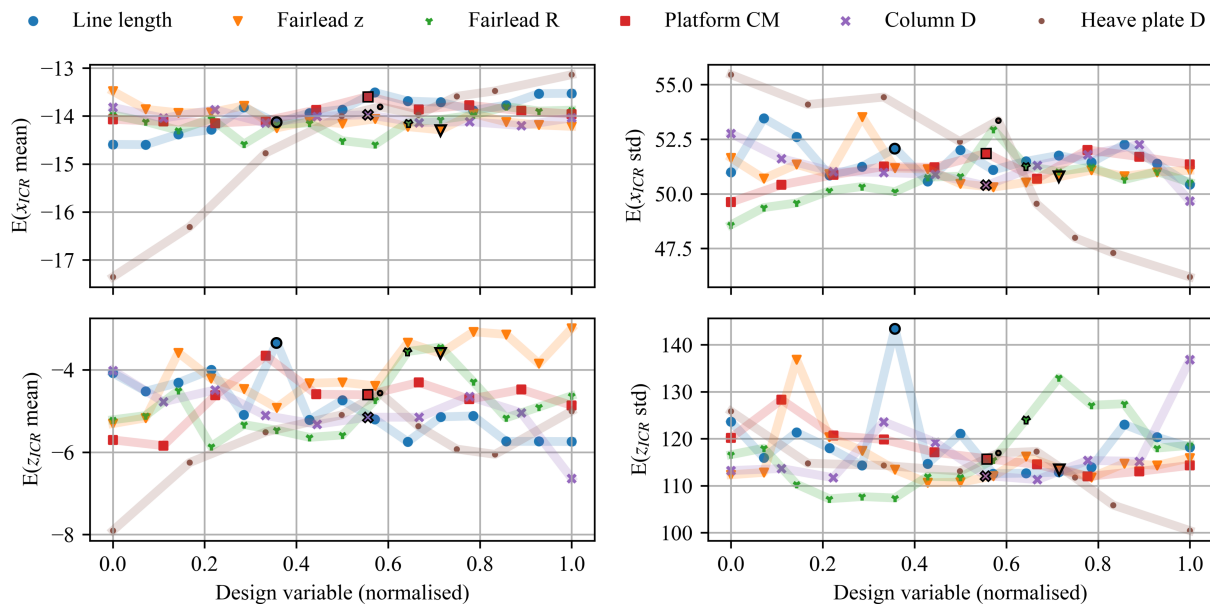
Figure 18. ICR statistics for different design variables one-at-a-time perturbations for a semisubmersible FOWT. Original design values marked with black outline.

To provide more quantitative insights, a sensitivity analysis was conducted using the data from Figures 17 and 18 to compute the Spearman correlation coefficient for each pair of design variables and ICR statistics (details in Sect. 2.2). As demonstrated in Figures 19 and 20, the sensitivity analysis confirmed the earlier observations. These quantitative results allow for ranking the design variables according to their impact on the ICR statistics, helping to identify which variables offer the greatest potential for ICR-driven design optimisation. This will be further explored in Sect. 6.
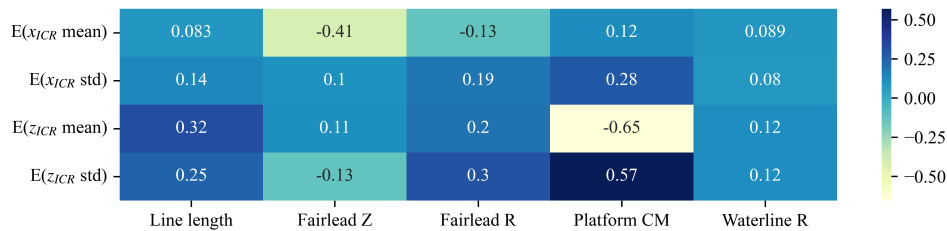
Figure 19. Correlation between the statistics of ICR and the design variables for the spar-type FOWT. See Figure A1 in Appendix A for correlations of all responses.
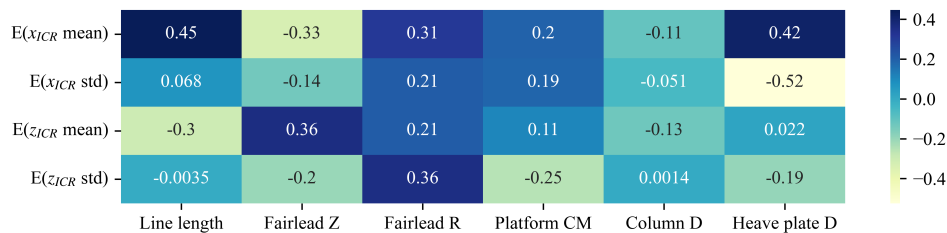
Figure 20. Correlation between the statistics of ICR and the design variables for the semisubmersible-type FOWT. See Figure A2 in Appendix A for correlations of all responses.

5 Responses sensitivity

To determine which responses of the spar FOWT can be improved by incorporating ICR in the design process, a sensitivity analysis was performed based on the full factorial design of experiments of the two most impactful design variables identified in Sect. 4 (vertical fairlead position and platform centre of mass), resulting in 64 variations of the floating systems.

Each design variation was simulated in 10 environmental conditions, and the results plotted refer to the average results weighted with the probability of occurrence of a given environmental condition, as explained in Sect. 2.3. The metrics considered included the nacelle fore-aft acceleration (referred to as NcIMUTAxs in tables and figures), blade root out-of-plane and tower base fore-aft bending moments (RootMyc1, TwrBsMyt), and the most loaded mooring line tension at the fairlead (FAIRTEN2), as well as the computed x and z coordinates of ICR (in the global inertial coordinate system). For each pair of responses, distribution statistics and the Spearman rank correlation coefficients were computed, as detailed in Sect. 4.

As illustrated in the correlation matrix in Figure 21, a significant negative correlation (-0.73 to -0.59) was observed between the standard deviation of the ICR horizontal coordinate and several responses, including nacelle acceleration and both the mean and standard deviation of tower base and blade root bending moments. A strong negative correlation was also observed between the mooring tension and the mean of x_{ICR} (-0.61 to -0.59). A weaker yet significant correlation (0.43 to 0.46) exists between the mean of x_{ICR} and the mean of the tower base and blade root loads. The standard deviation of z_{ICR} also exhibits a moderate correlation with these loads (0.41 to 0.45). Other statistics, such as skewness and kurtosis, were computed and analysed; however, they did not yield significant correlations and are therefore omitted for clarity. Similarly, the expected value is not included, as it was found to be very close to the mean of the distributions.
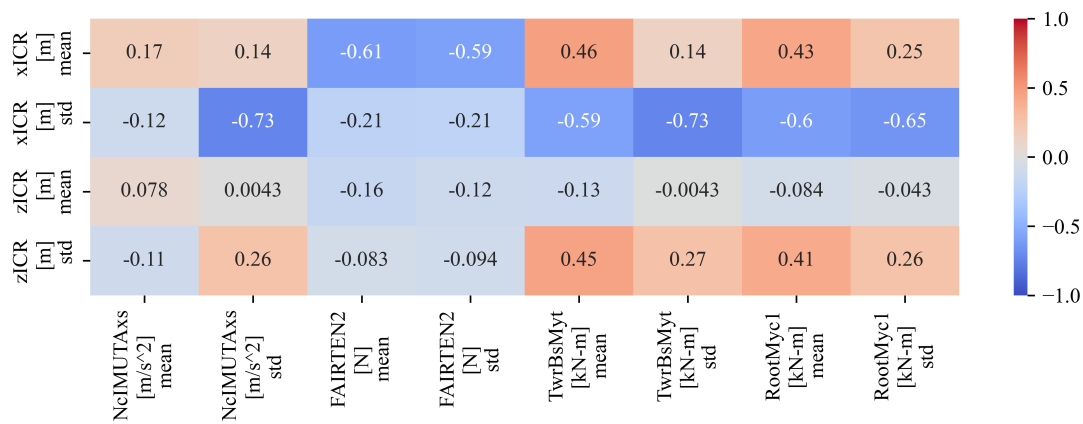
Figure 21. Spearman correlation between the statistics of ICR and the loads, obtained by varying the spar design features.

The same procedure was followed for the semisubmersible type of FOWT, investigating the responses of 512 designs of varying heave plate diameter, fairlead radius, and mooring line length according to the full factorial sampling strategy. As seen in Figure 22, the strongest correlation was found between the mean of z_{ICR} and all the responses considered but mooring tension (-0.86 to -0.83). A weaker correlation around $\rho = \pm 0.3$ was found between the mean of x_{ICR} and standard deviation of z_{ICR} and all responses of interest.

The presented correlation analysis provides information about the strength and direction of a monotonic relationship. However, it does not give specific information about the magnitude of the change of one parameter in response to a shift in another. Therefore, to assess the potential impact of the ICR on the responses of interest, the correlation results should be interpreted together with the information about the ranges of the responses' statistics, as provided in Table 10. By analysing the minimum, median, and maximum values, it can be concluded that the ranges of the responses highly correlated with ICR are sufficiently broad to be regarded as useful design metrics, offering adequate design flexibility. For example, the strong correlation between the mean of z_{ICR} and the standard deviation of the tower base bending moment, shown in Figure 22, is significant because both variables span meaningful ranges: the range of z_{ICR} from $-35.47\,\mathrm{m}$ to $-18.86\,\mathrm{m}$ corresponds to a tower base bending moment standard deviation range from $3.33\,\mathrm{MN\,m}$ to $6.48\,\mathrm{MN\,m}$.
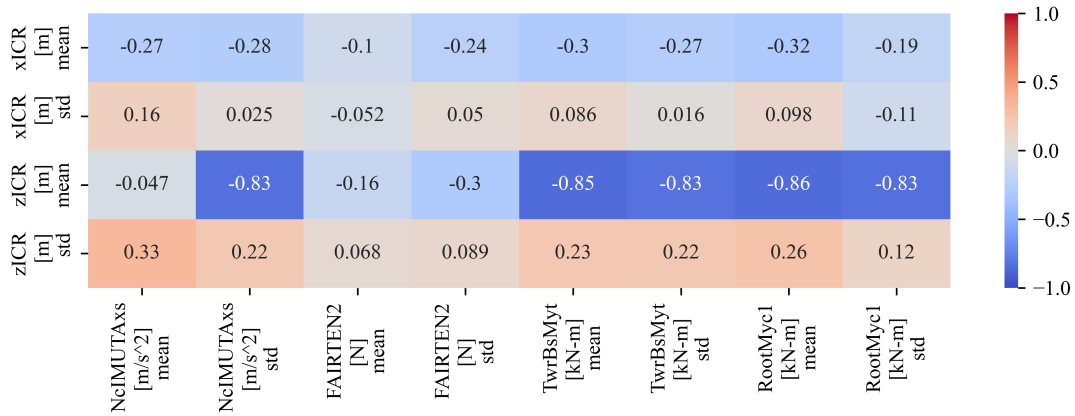
Figure 22. Spearman correlation between the statistics of ICR and the loads, obtained by varying the semisubmersible design features.

Table 10. Summary statistics of responses for spar and semisubmersible structures based on data used for the correlation analysis.

	Unit	Spar			Semisubmersible		
		Min	Median	Max	Min	Median	Max
NcIMUTAxs std	$\mathrm{m\,s^{-2}}$	0.06	0.08	0.12	0.06	0.08	0.12
FAIRTEN2 mean	kN	727.48	1650.63	10983.62	637.04	1276.43	2977.12
FAIRTEN2 std	kN	4.46	28.28	161.18	0.59	7.80	29.98
TwrBsMyt mean	$\mathrm{MN\,m}$	-0.95	21.20	82.80	-5.58	24.14	100.74
TwrBsMyt std	$\mathrm{MN\,m}$	1.69	2.79	4.49	3.33	4.35	6.48
RootMyc1 mean	$\mathrm{MN\,m}$	0.85	3.24	9.73	0.80	3.31	9.50
RootMyc1 std	$\mathrm{MN\,m}$	0.07	0.24	0.72	0.08	0.19	0.76
xICR mean	m	-2296.34	-14.27	-11.09	-8.43	-1.88	4.72
xICR std	m	38.85	49.98	11283.74	20.40	32.44	110.56
zICR mean	m	-681.28	-5.33	341.78	-35.47	-26.60	-18.86
zICR std	m	15.35	111.83	6697.62	5.97	13.84	46.28

6 Design Case Studies

325   The insights gained in the previous sections can be applied in design scenarios. The case studies presented here are defined based on the identification of the responses most sensitive to the ICR (i.e., which can be improved by adjusting ICR) (Sect. 5), and the design variables that have a significant impact on ICR and enable these improvements (Sect. 4). The first case study is done for the case of the spar-supported FOWT, and the second case focuses on the semisubmersible-type FOWT. The correlations used in the case studies are summarised in Figure 23 below and detailed in the subsequent sections.
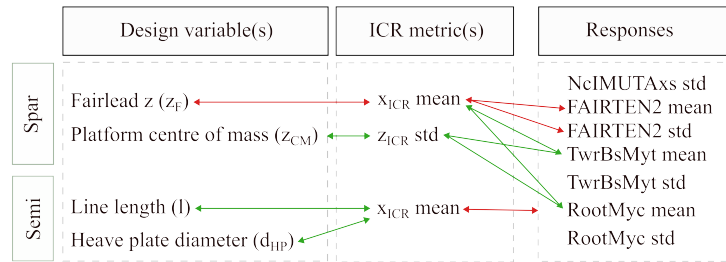
Figure 23. Case studies: design variables considered and their correlation with the ICR and responses statistics. Green/red arrows indicate a positive/negative correlation.

6.1 Spar sizing design case study

Given the observations made in Sect. 5 based on Figure 21, one major area would be particularly worth investigating in the context of design improvements through appropriate ICR "location". Namely, by maximising the standard deviation of the horizontal coordinate of ICR (i.e., by shifting it towards the positive x direction), one could simultaneously reduce the nacelle acceleration and the tower base and blade root bending moments. Lower nacelle acceleration is desired from the wind turbine's efficient and safe operation point of view; reducing the standard deviation of the tower and blade loads is important for system-wide fatigue damage reduction. However, for these improvements to be possible, it would be necessary to find a set of design variables correlated with the standard deviation of the horizontal coordinate of the ICR and the mean of the ICR coordinates. As can be seen in the correlation matrix in Figure 19 in Sect. 4, none of the variables considered gives any control over the standard deviation of x_{ICR}. Therefore, this metric cannot be modified in a design scenario.

Instead, the mean of x_{ICR} was seen to be strongly negatively correlated with the mean and standard deviation of the mooring loads and, at the same time, negatively correlated with the fairlead position. Therefore, it seems desirable to lower the fairlead position to increase the mean of x_{ICR} to decrease the mean and dynamic tension. However, the mean of x_{ICR} is also positively correlated with the mean of the tower and blade loads; therefore, shifting the ICR towards a position which improves the tension characteristics might increase the tower and the blade loads. This effect can be compensated for by simultaneously lowering the platform centre of mass to effectively reduce the tower and blade loads. Therefore, this case study will attempt to improve the mooring loads by varying two design variables: the vertical position of the fairlead and the platform centre of mass, keeping the tower base and blade roots mostly unaffected.

Figure 24 illustrates the design space in the form of $2D$ trends for the mean and standard deviation of the ICR coordinates and responses identified as correlated, for all combinations of the two selected design variables (full factorial design). While the sensitivity of the mean x_{ICR} to each variable is largely independent of the other variable (top left subplot), more interdependence is seen in the case of the standard deviation of z_{ICR}, where the rate of ICR increase with the centre of mass depends on the fairlead position and vice versa. Regarding the loads, the mooring line tension at the fairlead is significantly more sensitive

to variations in fairlead position than it is to the centre of mass. The impact of the two design variables on the tower base and blade root bending moments are more balanced, with both variables affecting the loads significantly.
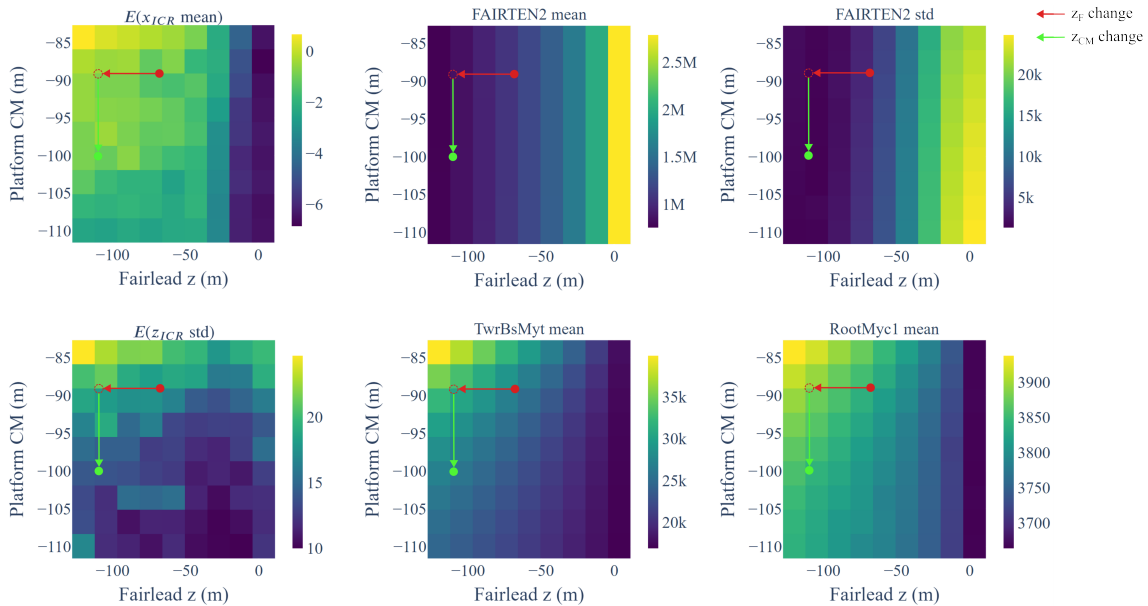
Figure 24. Design space visualisation: ICR and responses statistics as functions of two selected design variables for the spar-type FOWT.

As previously outlined in the diagram of Figure 23, and additionally illustrated in Figure 24, the design modifications follow the steps listed below:

- Lower the fairlead position to increase the mean x_{ICR} (top left plot, red arrow)

- This leads to a reduction of the mean and dynamic mooring tension (top middle and right plots, red arrows) and to an unfavourable increase in tower base and blade root bending moments (bottom middle and right plots, red arrows)

- Lower the platform centre of mass to lower the standard deviation of z_{ICR} (bottom left plot, green arrow)

- This brings the tower base and blade root loads back close to the original values while retaining the reduced mooring tension.

The extent of the variables adjustments is limited by practical considerations: the fairlead may not be practical to be constructed at the very bottom of the spar structure, and the centre of mass of the platform is limited by the ballast placement.

OpenFAST results of the original and the modified designs are compared in Table 11 and Figure 25. As expected, the most significant change was seen in the mooring loads, with 26 % and 69 % reductions in the mean and dynamic tension, respectively, improving both the ultimate strength and fatigue characteristics of the design. These changes were accompanied by shifting the mean of the body-fixed coordinate system ICR closer to the fairleads position. The softer mooring system resulted in vastly

increased mean surge offset of $21.73\,\text{m}$. Although this was a $50\,\%$ increase over the original design, the value is still reasonable
370    $(7\,\%$ of water depth assumed in this study). Importantly, the reduction of mooring loads was achieved without significantly compromising the other structural loads: the only response negatively affected was the tower base bending moment, which increased by less than $5\,\%$.

Table 11. Comparison of the original and the ICR-informed adjusted spar FOWT designs. Body-fixed frame ICR values in brackets.

Metric	Unit	Mean		Std	
		Original	Adjusted	Original	Adjusted
x_{ICR}	m	-2.13 (21.60)	-0.79 (12.63)	54.79 (33.35)	33.40 (54.80)
z_{ICR}	m	-28.69 (-23.27)	-24.31 (-28.86)	19.83 (15.36)	15.30 (19.58)
FAIRTEN2	N	1.09E+06	8.06E+05	4.24E+03	1.31E+03
TwrBsMyt	kN m	2.68E+04	2.64E+04	4.04E+03	4.21E+03
RootMyc1	kN m	3.83E+03	3.85E+03	2.37E+02	2.32E+02
Surge	m	13.93	21.73	0.12	0.13
Heave	m	-0.16	1.04	0.02	0.02
Pitch	°	1.62	1.53	0.06	0.06
NcIMUTAxs	m s^{-2}			0.11	0.11
Fairlead z	m	-70.00	-110.00	-70.00	-110.00
Platform z_{CM}	m	-89.92	-100.00	-89.92	-100.00
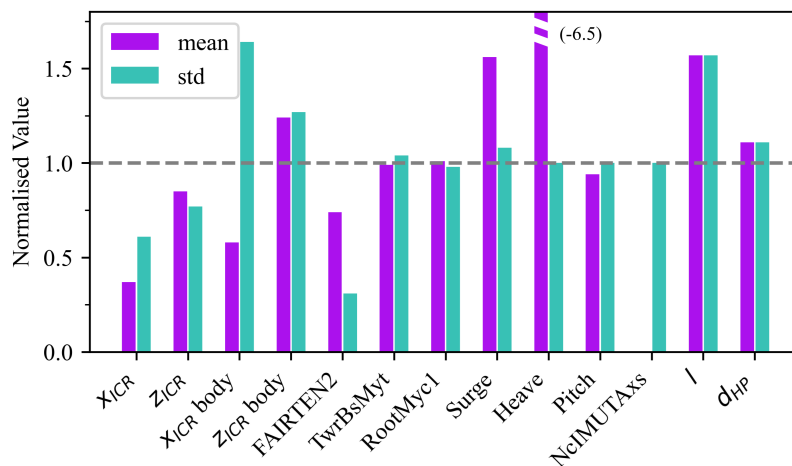
Figure 25. Comparison of the original and the modified spar FOWT designs. Values normalised with the original design values.

6.2 Semisubmersible sizing design case study

The second case study follows the procedure presented for the spar-type FOWT case, but this time, it is performed for the
375 semisubmersible-supported floating system. Based on the observations made in Sect. 5, the most promising design task would
be to adjust the structure's features to increase the mean of z_{ICR}, to decrease the nacelle acceleration, tower base, and blade
root loads simultaneously (and, to some extent, also reduce the mooring loads). However, by examining the correlation matrix
in Figure 20, it can be seen that the mean of z_{ICR} is only weakly correlated with the design variables considered. Although
the correlation of x_{ICR} with the responses of interest is significantly lower, the mean of x_{ICR} does show a strong correlation
380 with the design variables: mooring line length and heave plate diameter. Therefore, as outlined in the diagram of Figure 23,
and additionally illustrated in Figure 26, the design modifications follow the steps listed below:

- Increase the mooring line length and heave plate diameter to shift the mean x_{ICR} in the positive x-direction

- This should lead to a reduction in all responses of interest, most notably in the tower base and blade root mean loads.

Defining a single design metric (here, mean of x_{ICR}) that accounts for multiple metrics (here, nacelle acceleration, mooring,
385 tower, and blade root loads) might be beneficial in design optimisation scenarios, as it reduces the size of the optimisation
problem, potentially leading to a less time-consuming and more robust optimisation process. Note that this case study only
attempts a "manual" design sizing for simplicity and clear demonstration.
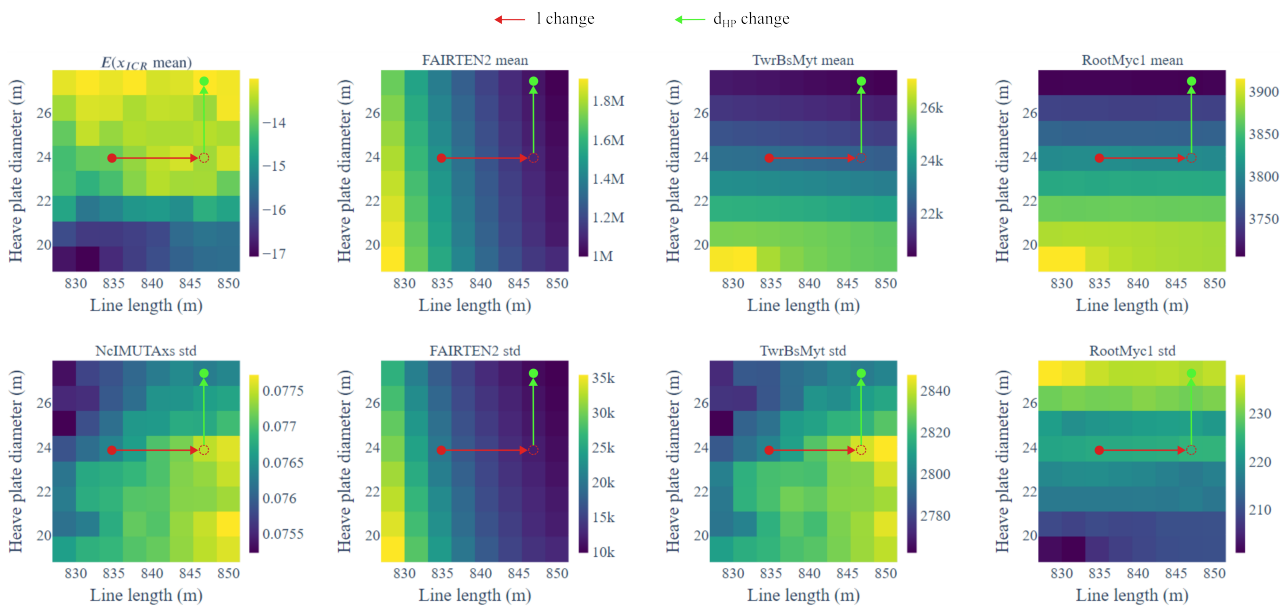
Figure 26. Design space visualisation: ICR and responses statistics as functions of two selected design variables for the semi-type FOWT.

The comparison of the original and the modified designs in Table 12 and Figure 27 show a significant reduction in all loads
except for the dynamic blade root loads, which increased slightly.

Table 12. Comparison of the original and the ICR-informed adjusted semisubmersible FOWT designs. Body-fixed frame ICR values in brackets.

Metric	Unit	Mean		Std	
		Original	Adjusted	Original	Adjusted
x_{ICR}	m	-13.60 (-7.29)	-13.11 (-0.75)	51.9 (51.75)	45.54 (45.44)
z_{ICR}	m	-3.97 (-4.22)	-4.99 (-10.31)	117.17 (117.25)	98.64 (98.68)
FAIRTEN2	N	1.44E+06	1.05E+06	1.96E+04	1.07E+04
TwrBsMyt	kN m	2.27E+04	2.05E+04	2.81E+03	2.80E+03
RootMyc1	kN m	3.80E+03	3.70E+03	2.21E+02	2.33E+02
Surge	m	6.21	12.28	0.10	0.10
Heave	m	-0.02	-5.18	0.03	0.02
Pitch	°	0.94	0.63	0.07	0.06
NcIMUTAxs	$m\,s^{-2}$			0.08	0.08
Line length	m	835.5	847	835.5	847
Heave plate d	m	24	27.35	2	27.35
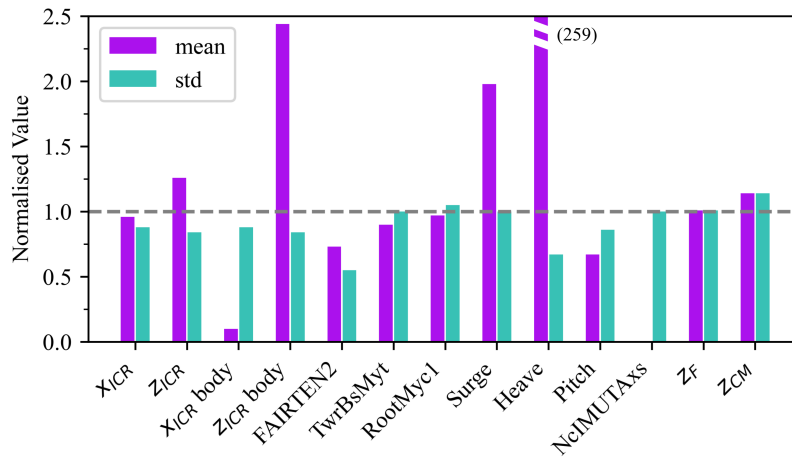
Figure 27. Comparison of the original and the modified semisubmersible FOWT designs. Values normalised with the original design values.

This case study clearly illustrates the issue discussed earlier in Sect. 4. Specifically, when adjusting design variables, multiple characteristics of the floating system can change as a consequence. Notably, significant alterations to the draft may occur due to modifications in the underwater geometry of the floating platform and its displacement volume. Such changes may be undesirable, especially when the draft is a critical design parameter established early in the design process, often constrained by port depth and manufacturing and assembly capabilities. To address this concern, an additional step was incorporated in this case study: the system's total mass was reduced to restore the draft close to its original value (mass distribution was not changed in this simple exercise). As detailed in Table 12, the loads of the modified re-ballasted design still show improvement

over the original design. However, these improvements are more modest, indicating that the increased draft was a significant, though not the sole, contributor to the substantial reductions observed initially.

400   To achieve a draft close to the original value, a significant mass (ballast water) reduction was necessary (14 %). Alternatively, to maintain the same draft, the change in underwater volume caused by adjusting the size of the heave plates could be compensated by modifying the diameters of the offset columns, keeping the ballast mass unchanged. This was done based on the original undisplaced displacement volume and draft. As demonstrated in Table 13, the volume compensation yielded results similar to re-ballasting the platform, resulting in slightly better dynamic mooring tension but a slightly worse standard deviation for the tower base and blade root loads.

Table 13. Comparison of the original and the ICR-informed adjusted semisubmersible FOWT designs, considering ballasting and volume compensation strategies. Body-fixed frame ICR values in brackets. *Re-vol.* – Volume-compensated; *Re-bal.* – Re-ballasted.

Metric	Unit	Mean			Std		
		Original	Re-vol.	Re-bal.	Original	Re-vol.	Re-bal.
x_{ICR}	m	-13.60 (-7.29)	-13.43 (-2.02)	-14.15 (-2.33)	51.9 (51.75)	47.32 (47.19)	49.43 (49.31)
z_{ICR}	m	-3.97 (-4.22)	-7.41 (-9.29)	-7.51 (-8.21)	117.17 (117.25)	103.85 (103.91)	112.88 (112.93)
FAIRTEN2	N	1.44E+06	1.06E+06	1.10E+06	1.96E+04	1.13E+04	1.23E+04
TwrBsMyt	kN m	2.27E+04	2.13E+04	2.14E+04	2.81E+03	2.88E+03	2.82E+03
RootMyc1	kN m	3.80E+03	3.76E+03	3.79E+03	2.21E+02	2.25E+02	2.26E+02
Surge	m	6.21	11.28	11.68	0.10	0.11	0.11
Heave	m	-0.02	-1.71	-0.51	0.03	0.02	0.03
Pitch	°	0.94	0.73	0.73	0.07	0.07	0.06
NcIMUTAxs	m s^{-2}				0.08	0.08	0.08
Line length	m	835.5	847	847	835.5	847	847
Heave plate d	m	24	27.35	27.35	24	27.35	27.35
Offset column d	m	12	8.38	12	12	8.38	12
Platform mass	kg	1.35E+07	1.35E+07	1.16E+07	1.35E+07	1.35E+07	1.16E+07

405   7   Conclusions

This study investigated the Instantaneous Centre of Rotation (ICR) of spar and semisubmersible Floating Offshore Wind Turbines (FOWTs) through time domain analysis. It examined the dependence of ICR on complex environmental loading conditions and design features of the support structure, as well as the relationships between the ICR statistics and key FOWT responses.

410   The statistics of ICR coordinates under increasingly complex external loading conditions were analysed, isolating the impacts of mean wind speed, shear, turbulence intensity, regular wave frequency, irregular waves, and current speed. The results indicated that the ICR coordinates of FOWTs operating in realistic environmental conditions exhibit significant variability, fol-

lowing a heavy-tailed, sharp-peaked distribution with a high likelihood of extreme values. Notably, at a moderate confidence level of $60\,\%$, the range of the vertical ICR coordinate of the spar-type FOWT was approximately $80\,\mathrm{m}$, indicating that precise placement of the ICR is challenging in complex environments.

To inform practical design applications, we explored which design variables could be adjusted to influence ICR statistics and how these statistics affected key responses. We identified the design variables most correlated with ICR: the platform's center of mass and the vertical position of the fairlead for the spar, and the mooring line length and heave plate diameter for semisubmersible FOWT. A full factorial design of experiments revealed significant correlations between ICR and the responses of interest: nacelle acceleration, tower base fore-aft bending moment, blade root out-of-plane moment, and mooring line tension. For the spar system, these were significantly correlated with the horizontal ICR coordinate, and for the semisubmersible, the highest correlation was found with the mean of the ICR coordinates.

Sets of highly correlated design variables, ICR statistics, and responses were selected and used to formulate case studies, where 2D design trends were visualised and analysed to identify preferred design directions. In the spar FOWT case, the fairlead position was adjusted to shift the mean of x_{ICR} closer to the fairleads. Although with the design modifications considered, it was impossible to align the mean ICR with the fairleads, moving the ICR in that direction significantly reduced mean and dynamic mooring loads. This adjustment had a negative impact on the tower and blades loads, which were mitigated by shifting the platform's centre of mass, thereby shifting the standard deviation of z_{ICR} and restoring these loads to their original levels. The semisubmersible case study demonstrated a key advantage of using ICR as a design metric: modifying a single ICR statistic (the mean of z_{ICR}) improved all response variables simultaneously. This shows that employing ICR as a design criterion provides a single objective that effectively addresses multiple concerns, leading to more efficient optimisation problem formulation.

8 Future work

To generalise the conclusions to any floating system, further research should investigate how the characteristics of externally applied loads—such as amplitude, point of application, distribution, and frequency—along with the system's inertial and restoring properties affect the motion response, ICR, and structural loads. This research should abstract from platform geometry and environmental conditions, focusing instead on the fundamental load-response interactions. Additionally, the parametrisation of the FOWT support structure should be refined to allow more control over the designs and the ICR, in particular, the separation of the semisubmersible columns, which is an important design feature overlooked in this study. Conducting the analysis in the design load cases commonly considered at the concept design/feasibility study stage would be insightful. Lastly, a more efficient, frequency domain approach to computing the ICR would benefit initial design space screening and optimisation tasks.

Appendix A

This appendix presents the correlation matrices (Spearman correlation) between the design variables and the responses of interest for the spar (Figure A1) and semisubmersible (Figure A2) FOWTs.
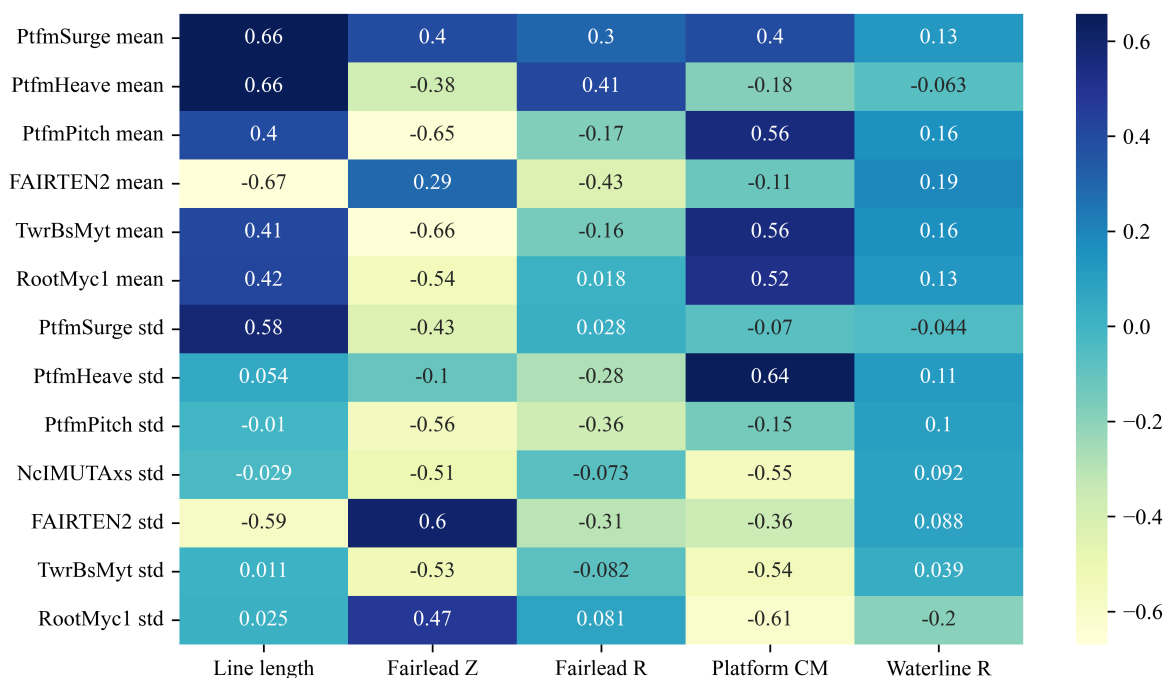
Figure A1. Correlation matrix between the design variables and the responses of interest for the spar design.

445 *Author contributions.* KP, MC, JJ, GB, MH, DZ conceptualised the study. KP developed the methodology and performed formal analysis, investigation, visualisation and original draft preparation. MC, JJ, GB, MH, DZ, AC provided supervision. All authors contributed to the draft review & editing.

Competing interests. Some authors are members of the editorial board of this journal.

Acknowledgements. This work was supported by the University of Strathclyde REA 2024.
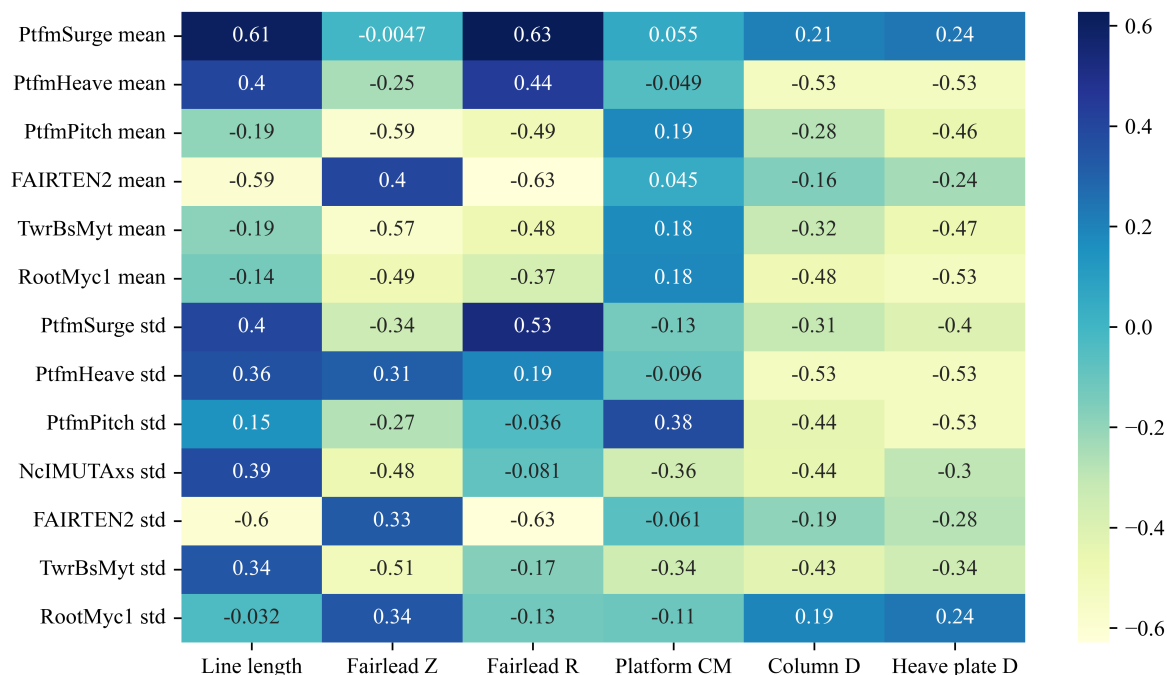
Figure A2. Correlation matrix between the design variables and the responses of interest for the semisubmersible design.

References

Costa, D., Fernandes, A. C., Sales Junior, J. S., and Asgari, P.: Instantaneous Center of Rotation in Pitch Response of a FPSO Submitted to Head Waves, vol. Volume 7A: Ocean Engineering of *International Conference on Offshore Mechanics and Arctic Engineering*, 2018.

Costa, D., Fernandes, A. C., and Sales Junior, J. S.: Further study on the Instantaneous Rotation Center in Pitch and its distribution in space for a moored vessel submitted to head regular waves, Ocean Engineering, 218, 2020a.

Costa, D., Sales Junior, J. S., and Fernandes, A. C.: Instantaneous Center of Rotation of a Vessel Submitted to Oblique Waves, vol. Volume 6B: Ocean Engineering of *International Conference on Offshore Mechanics and Arctic Engineering*, 2020b.

Eliassen, L.: Aerodynamic Loads on a Wind Turbine Rotor in Axial Motion, Ph.D. thesis, University of Stavanger, Stavanger, Norway, 2015.

Fernandes, A. C., Asgari, P., and Soares, A. R.: Asymmetric roll center of symmetric body in beam waves, Ocean Engineering, 112, 66–75, 2016.

Hall, M. and Goupee, A.: Validation of a lumped-mass mooring line model with DeepCwind semisubmersible model test data, Ocean Engineering, 104, 2015.

Haslum, H. A. and Faltinsen, O. M.: Simplified methods applied to nonlinear motion of spar platforms (A thesis submitted in partial fulfilment of the requirements for the degree of Doktor Ingenipr. Trondheim), 2000.

IEC: Technical Specification IEC 61400-3:2009. Wind turbines - Part 3: Design requirements for offshore wind turbines, 2009.

IEC: Technical Specification IEC 61400-3-2. Wind energy generation systems - Part 3-2: Design requirements for floating offshore wind turbines, 2019.

Jonkman, J.: Definition of the Floating System for Phase IV of OC3, Tech. rep., National Renewable Energy Laboratory (NREL), 2010.

Jonkman, J., Butterfield, S., Musial, W., and Scott, G.: Definition of a 5-MW Reference Wind Turbine for Offshore System Development, 2009.

470 Kaptan, M., Skaare, B., Jiang, Z., and Ong, M. C.: Analysis of spar and semi-submersible floating wind concepts with respect to human exposure to motion during maintenance operations, Marine Structures, 83, 2022.

Lee, C. H. and Newman, J. N.: WAMIT User Manual, Versions 6.4, Tech. rep., Massachusetts Institute of Technology, 2006.

Lemmer, F., Yu, W., Müller, K., and Cheng, P. W.: Semi-submersible wind turbine hull shape design for a favorable system response behavior, Marine Structures, 71, 2020.

475 Meriam, J, L. and Kraige, L, G.: Engineering Mechanics, Volume 2, Dynamics, John Wiley & Sons, Inc., 7th edn., 1993.

NREL: OpenFAST, v3.5, https://github.com/openfast/openfast/, 2024.

Patryniak, K., Collu, M., and Coraddu, A.: Rigid body dynamic response of a floating offshore wind turbine to waves: Identification of the instantaneous centre of rotation through analytical and numerical analyses, Renewable Energy, 218, 2023.

Souza, F., Anderson, R., Oliveira, A., and Fernandes, A.: Influência do Centro de Rotação através de Ensaios de Decaimento no Movimento
480 de Balanço Transversal de Cascos Típicos de FPSO (in Portuguese), XXIV Congresso Nacional de Transportes Marítimos e Construção Naval e Offsh, 2012.

Standing, R.: Prediction Of Viscous Roll Damping And Response Of Transportation Barges In Waves, International Ocean and Polar Engineering Conference, 1991.

Stewart, W. P. and Ewers, W. A.: Wave Induced Motions of Marine Deck Cargo Barges, in: Second International Conference on Behaviour
485 of Off-Shore Structures, BOSS'79, Imperial College, London, 1979.